

Constraints on the abundance of primordial black holes with different mass distributions from lensing of fast radio bursts

Huan Zhou,¹ Zhengxiang Li,^{2*} Zhiqi Huang,^{1†} He Gao,² Lu Huang¹

¹*School of Physics and Astronomy, Sun Yat-sen University, Zhuhai, 519082, China*

²*Department of Astronomy, Beijing Normal University, Beijing 100875, China*

Accepted XXX. Received YYY; in original form ZZZ

ABSTRACT

Primordial black holes (PBHs) has been considered to form a part of dark matter for a long time but the possibility has been poorly constrained over a wide mass range, including the stellar mass range ($1 - 100 M_{\odot}$). However, due to the discovery of merger events of black hole binaries by LIGO-Virgo gravitational wave observatories, the interest for PBHs in the stellar mass window has been aroused again. Fast radio bursts (FRBs) are bright radio transients with millisecond duration and very high all-sky occurrence rate. Lensing effect of these bursts has been proposed as one of the optimal probes for constraining the abundance of PBHs in the stellar mass range. In this paper, we first investigate constraints on the abundance of PBHs from the latest 593 FRB observations for both the monochromatic mass distribution and three other popular extended mass distributions related to different formation mechanisms of PBHs. It is found that constraints from currently public FRB observations are relatively weaker than those from existing gravitational wave detections. Furthermore, we forecast constraining power of future FRB observations on the abundance of PBHs with different mass distributions of PBHs and different redshift distributions of FRBs taken into account. Finally, We find that constraints of parameter space on extended mass distributions from $\sim 10^5$ FRBs with $\Delta t \leq 1$ ms would be comparable with what can be constrained from gravitational wave events. It is foreseen that upcoming complementary multi-messenger observations will yield considerable constraints on the possibilities of PBHs in this intriguing mass window.

Key words: Primordial black holes, Fast radio bursts, Gravitational lensing

1 INTRODUCTION

The detection of the first gravitational wave (GW) event from binary black hole (BH) merger heralds the arrival of the GW astronomy era (Abbott et al. 2016). Soon after the first detection, several research groups independently pointed out that these BHs might be primordial, i.e. primordial black holes (PBHs), and the inferred merger rate can be explained by the merger of PBHs (Bird et al. 2016; Sasaki et al. 2016; Clesse & García-Bellido 2017). PBHs can be formed in the early universe through several mechanisms, including gravitational collapse of primordial density perturbations (Hawking 1971; Carr & Hawking 1974; Carr 1975) arising from quantum fluctuation (Clesse & García-Bellido 2015; Pi et al. 2018; Ashoorioon et al. 2021; Fu et al. 2019; Chen & Cai 2019; Motohashi et al. 2020), bubble collisions (Hawking et al. 1982), cosmic string (Hawking 1989; Hogan 1984), and domain wall (Caldwell et al. 1996). Diversity of formation

mechanism means that PBHs might have different evolutionary history with respect to astrophysical black holes that are produced from the demise of massive stars. In principle, the mass of PBHs can range from the Planck mass (10^{-5} g) to the level of the black hole in the center of the galaxy.

Moreover, PBHs have been a field of great astrophysical interest because they are often considered to make up a part of dark matter which accounts for about one fourth of the total energy density of the universe. The scenario that the universe mainly consists of dark matter and dark energy ($\sim 70\%$) is well consistent with many cosmological observations. However, we still know little about the constituent of dark matter, especially in small scales. Observational searches for the possibility of PBHs as dark matter candidates have been conducted intensively and continuously over several decades. Numerous methods have been proposed to constrain the fraction of PBHs in dark matter $f_{\text{PBH}} = \Omega_{\text{PBH}}/\Omega_{\text{DM}}$ at present universe. We can see Sasaki et al. (2018); Green & Kavanagh (2021) for a review in various mass windows. These constraints include direct observational effects: gravitational lensing (Niikura et al. 2019; Griest et al. 2013; Niikura et al.

* E-mail: zxli918@bnu.edu.cn

† huangzhq25@mail.sysu.edu.cn

2019a; Tisserand et al. 2007; Alcock et al. 2001; Zumalacarregui & Seljak 2018; Mediavilla et al. 2017), dynamical effects on ultrafaint dwarf galaxies (Brandt 2016; Koushiappas & Loeb 2017), non-detections of stochastic GW (Wang et al. 2018; Clesse & García-Bellido 2017; Chen & Huang 2020; De Luca et al. 2020; Hütsi, et al. 2021), disruption of white dwarfs (Graham et al. 2015), and the accretion effects on cosmic microwave background (Ali-Haimoud, & Kamionkowski 2017; Aloni et al. 2017; Chen et al. 2016; Poulin et al. 2017; Bernal et al. 2017), (extra)galactic γ -ray backgrounds (Carr et al. 2016; Laha 2019; DeRocco & Graham 2019; Laha et al. 2020; Dasgupta et al. 2020) can be used to constraints on the PBHs lighter than $\sim 10^{15}$ g that would have already evaporated through the Hawking radiation (Carr et al. 2010). Indirect observational effects, i.e. null detection of scalar-induced GW (Chen et al. 2020) and cosmic microwave background (CMB) spectral distortions from the primordial density perturbations (Carr & Lidsey 1993; Carr et al. 1994) have been proposed to constrain the abundance of PBHs. In addition to these available probes, some other constraints from future observations, i.e. gravitational lensing of GW (Liao et al. 2020; Diego 2020; Urrutia & Vaskonen 2021), gamma-ray bursts (Ji et al. 2018), and 21 cm signals (Hektor et al. 2018; Clark et al. 2018; Halder & Banerjee 2021), have been proposed.

PBHs within the mass range $1 - 100 M_{\odot}$ (stellar mass range) have attracted growing attention because of the recent detection of GW from binary black hole merger (Abbott et al. 2016) and in result detection of GW bursts from merges of compact object binaries has considered as one of the most promising ways to study the mass distribution of PBHs. Meanwhile, PBHs in the stellar mass range also could be detected with the gravitational lensing effect of prolific transients with millisecond duration, e.g. fast radio bursts (FRBs).

FRBs are bright radio transients with short duration of few milliseconds. This mysterious burst was first reported by Lorimer et al. (2007) and so far several hundred public FRBs are available¹. Most FRBs are apparently one-off, meanwhile there are also dozens of repeaters. The observed extremely excess dispersion measure (DM: proportional to the number density of free electron along the line of sight of radio emission) of FRBs discovered at the early stage indicates their cosmological origin (Lorimer et al. 2007; Thornton et al. 2013) and it has been soon verified by the localizing the first repeater FRB121102 to a nearby dwarf galaxy (Tendulkar et al. 2017; Chatterjee et al. 2017; Marcote et al. 2017). According to the detection rate and the field of view of radio telescopes, a high event rate of this kind of mysterious phenomenon ($\sim 10^3$ to 10^5 per day all sky) has been inferred (Thornton et al. 2013; Champion et al. 2016; Niu et al. 2021). For instance, it was estimated that Canadian Hydrogen Intensity Mapping Experiments (CHIME) will detect $\sim 10^4$ FRBs per year, of which $\sim 10^3$ FRBs with redshift information will be probed (Connor et al. 2016). Although the radiation mechanism and progenitors of these mysteries are still intensively debated², some unique and useful obser-

vational properties of FRBs, including clean temporal shape, short temporal duration, cosmological origin, and high all-sky event rate have been proposed as promising cosmological and astrophysical probes, such as testing fundamental physics (Wei et al. 2015; Wu et al. 2016), constraining cosmological models (Gao et al. 2014; Zhou et al. 2014; Walters et al. 2018; Zhao et al. 2020), baryon census (Deng & Zhang 2014; Muñoz & Loeb 2018; Macquart et al. 2020; Li et al. 2019, 2020), reionization history of universe (Linder 2020; Bhattacharya, Kumar, & Linder 2021; Beniamini et al. 2021), millilensed lensed FRBs for probing compact dark matter (Muñoz et al. 2016; Wang & Wang 2018; Liao et al. 2020; Laha 2020; Zhou et al. 2021), galaxy lensing time delay variations for probing the the motion of the FRB source (Dai & Lu 2017), and time delay distances of strongly lensed FRBs for precisely measuring the expansion rate and curvature of the universe (Li et al. 2018; Wucknitz, Spitler, & Pen 2020).

In this paper, following the method proposed in Liao et al. (2020); Laha (2020), we concentrate on constraining the abundance of PBHs in the stellar mass range from lensing of FRBs. First, with the monochromatic mass distribution (MMD) and three other extended mass distributions (EMDs), we derive constraints on the the abundance of PBHs from the null search result of the latest FRB observations. Moreover, we investigate constraints on the PBH properties from near future FRB observations by taking the detection ability of already running and upcoming telescopes and possible redshift distribution of FRBs into consideration. Finally, comparisons between constraints on the PBH properties from FRBs observations and the ones obtained from GW detection are presented to explore the possibility of deriving joined constraints on PBHs from upcoming multi-messenger observations.

This paper is organized as follows. We review the theory of FRBs lensing by PBHs with different mass functions in Sec. 2. In Sec. 3 we briefly introduce the latest FRB observations and present the constraints on PBHs from them for both MMD and EMDs. Sec. 4 shows constraints from upcoming FRB observations on parameter space of PBHs with different EMD, as well as comparisons between the constraints on PBHs from the merger rate of PBH binaries in view of GW detection with the ones from near future FRB observations. Finally, we conclude and discuss in Sec. 5.

2 LENSING OF FRBS

The theory of gravitational lensing is a well-studied phenomenon and is used as an observational tool in astrophysics to probe objects which are too faint to be detected by conventional means. It has been proposed for probing PBHs in the universe for a long time. For a lensing system, Einstein radius is one of the characteristic parameters and, taking the intervening lens as a point mass, it is given by

$$\theta_E = 2\sqrt{\frac{GM_{\text{PBH}}D_{\text{LS}}}{c^2D_{\text{L}}D_{\text{S}}}} \approx (3 \times 10^{-6})'' \left(\frac{M_{\text{PBH}}}{M_{\odot}}\right)^{\frac{1}{2}} \left(\frac{D}{\text{Gpc}}\right)^{-\frac{1}{2}}, \quad (1)$$

where G and c represent the gravitational constant and the speed of light, respectively. In addition, $D = D_{\text{L}}D_{\text{S}}/D_{\text{LS}}$ is effective lensing distance, where D_{S} , D_{L} and D_{LS} represent

¹ <https://www.wis-tns.org>

² The recent detection of a Galactic FRB in association with a soft gamma-ray repeater suggests that magnetar engines can produce at least some (or probably all) FRBs (Zhang 2020; CHIME/FRB Collaboration, 2020; Bochenek et al. 2020; Lin et al. 2020).

the angular diameter distance to the source, to the lens, and between the source and the lens, respectively. Although the angular resolution for some repeaters with very long baseline array (VLBA) could reach a high level, e.g. $\sim (10^{-2})''$ of VLBA observations for FRB 121102 (Spitler et al. 2016; Chatterjee et al. 2017; Tendulkar et al. 2017; Marcote et al. 2017), it is just possible to distinguish multiple images of an FRB lensed by intervening objects with mass greater than $10^8 M_\odot$. Another characteristic parameter for a lensing system is the time delay between lensed signals and it can be approximately expressed as,

$$\Delta t \approx 1 \text{ ms} \left(\frac{M_{\text{PBH}}}{30 M_\odot} \right). \quad (2)$$

Therefore, for lensing systems where PBHs with mass in $1 - 100 M_\odot$ acting as deflectors, the time delay between multiple images is $\sim 0.1 - 1$ ms and is accurately determined by,

$$\Delta t(M_{\text{PBH}}, z_L, y) = \frac{4GM_{\text{PBH}}}{c^3} (1 + z_L) \left[\frac{y}{2} \sqrt{y^2 + 4} + \ln \left(\frac{\sqrt{y^2 + 4} + y}{\sqrt{y^2 + 4} - y} \right) \right], \quad (3)$$

where the normalized impact parameter $y = \beta/\theta_E$ is defined as the ratio of the angular impact parameter to the angular Einstein radius, z_L is the lens redshift. Δt must be larger than the width (w) of the observed signal to resolve lensed echoes. This requires y larger than a certain value $y_{\text{min}}(M_{\text{PBH}}, z_L, w)$ according to Eq. 3. The lensing cross section due to a PBH lens is given by an annulus between the maximum and minimum impact parameters,

$$\sigma(M_{\text{PBH}}, z_L, z_S, w) = \frac{4\pi GM_{\text{PBH}} D_L D_{LS}}{c^2 D_S} [y_{\text{max}}^2(R_f) - y_{\text{min}}^2(M_{\text{PBH}}, z_L, w)], \quad (4)$$

where R_f is the flux ratio. It is defined as the absolute value of the ratio of the magnifications μ_+ and μ_- of both images,

$$R_f \equiv \left| \frac{\mu_+}{\mu_-} \right| = \frac{y^2 + 2 + y\sqrt{y^2 + 4}}{y^2 + 2 - y\sqrt{y^2 + 4}} > 1. \quad (5)$$

The maximum value of normalized impact parameter can be found by requiring that the flux ratio of two lensed images is smaller than a critical value $R_{f,\text{max}}$,

$$y_{\text{max}}(R_{f,\text{max}}) = R_{f,\text{max}}^{1/4} - R_{f,\text{max}}^{-1/4}, \quad (6)$$

to ensure that both signals are detectable. Here, following Muñoz et al. (2016), we take $R_{f,\text{max}} = 5$ for cases when we study lensing of the whole sample of all currently public FRBs. For a single source, the optical depth for lensing due to a single PBH is

$$\tau(M_{\text{PBH}}, f_{\text{PBH}}, z_S, w) = \int_0^{z_S} d\chi(z_L) (1 + z_L)^2 n_L(f_{\text{PBH}}) \sigma(M_{\text{PBH}}, z_L, z_S, w) = \frac{3}{2} f_{\text{PBH}} \Omega_{\text{DM}} \int_0^{z_S} dz_L \frac{H_0^2}{cH(z_L)} \frac{D_L D_{LS}}{D_S} (1 + z_L)^2 [y_{\text{max}}^2(R_{f,\text{max}}) - y_{\text{min}}^2(M_{\text{PBH}}, z_L, w)], \quad (7)$$

where n_L is the comoving number density of the lens, $H(z_L)$ is the Hubble parameter at z_L , H_0 is the Hubble constant and we use the value estimated from the latest CMB observations (Planck Collaboration, 2020) in our following analysis, f_{PBH} represents the fraction of PBHs in dark matter,

and Ω_{DM} is the present density parameter of dark matter. In order to find the total lensing optical depth, one has to integrate the optical depth in Eq. 7. At present, the latest observations of FRB consist of 593 well-identified events, which provides a statistically meaningful sample. According to the definition, the expected number of lensed FRBs in currently public observations is approximately equivalent to the sum of the lensing optical depths of all FRBs,

$$N_{\text{lensed FRB}} = \sum_{i=1}^{N_{\text{total}}} \tau_i(M_{\text{PBH}}, f_{\text{PBH}}, z_{S,i}, w_i). \quad (8)$$

It should be pointed out that the above formalism is only valid for the simple but often used MMD,

$$P(m, M_{\text{PBH}}) = \delta(m - M_{\text{PBH}}), \quad (9)$$

where $\delta(m - M_{\text{PBH}})$ represents the δ -function at the mass M_{PBH} . In fact, there are some EMDs which have more robust physical motivations. Therefore, it is important and necessary to derive constraints on PBH with some theoretically motivated EMDs, which are closely related to formation mechanisms of PBHs. In this paper, we take three EMDs into consideration, i.e. the extend power-law mass function, the log-normal mass function, and the critical collapse mass function. Concretely, the extend power-law mass function is parametrized as (Laha 2020; Bellomo et al. 2018),

$$P(m, M_{\text{min}}, M_{\text{max}}, \gamma) = \frac{\mathcal{N}_{\text{pl}}}{M^{1-\gamma}} \Theta(M_{\text{max}} - m) \Theta(m - M_{\text{min}}), \quad (10)$$

where the mass range of the distribution is bordered by the minimum mass, M_{min} , and the maximum mass, M_{max} . The exponent of the power law is denoted by γ . The normalization factor \mathcal{N}_{pl} is,

$$\mathcal{N}_{\text{pl}} = \begin{cases} \frac{\gamma}{M_{\text{max}}^\gamma - M_{\text{min}}^\gamma}, & \gamma \neq 0, \\ \frac{1}{\ln(M_{\text{max}}/M_{\text{min}})}, & \gamma = 0, \end{cases} \quad (11)$$

where the exponent γ is determined by the formation epoch of the PBH, and the natural range of exponent γ is $\gamma \in (-1, 1)$, which corresponds to the equation of state $\omega \in (-1/3, 1)$. Interesting values of the exponent are $\gamma = -0.5$ and $\gamma = 0$, corresponding to formation during radiation and matter dominated, respectively. We take γ as a free parameter with prior $\gamma \leq 0$. This mass function can arise if the PBHs are generated by scale-invariant density fluctuations or from the collapse of cosmic strings. The log-normal mass function is (Hütsi, et al. 2021; Carr et al. 2017; Bellomo et al. 2018):

$$P(m, \sigma, m_c) = \frac{1}{\sqrt{2\pi}\sigma m} \exp\left(-\frac{\ln^2(m/m_c)}{2\sigma^2}\right), \quad (12)$$

where m_c and σ denote the peak mass of $mP(m)$ and the width of mass spectrum, respectively. This mass function is often a good approximation if the PBHs produced from a smooth symmetric peak in the inflationary power spectrum, and it had been demonstrated numerically in Green (2016) and analytically in Kannike et al. (2017) for the case where the slow-roll approximation holds. Therefore, it is a representative of a large class of extend mass functions. A critical collapse mass function is (Carr et al. 2017; Hütsi, et al. 2021;

Carr et al. 2016):

$$P(m, \alpha, M_f) = \frac{\alpha^2}{M_f^{1+\alpha} \Gamma(1/\alpha)} m^\alpha \exp\left(-\left(\frac{m}{M_f}\right)^\alpha\right), \quad (13)$$

where M_f is a mass-scale which corresponds to the horizon mass at the collapse epoch, and $\alpha \sim 3$ is a universal exponent which is related to the critical collapse of radiation. In this case, the mass spectrum can extend down to arbitrarily low masses, but there is an exponential upper cut-off at a mass-scale M_f . We take α as a free parameter ranging from 1.5 to 3 in our analysis. This mass function is supposed to be closely related to PBHs originating from density fluctuations with a δ -function power spectrum.

For the above-mentioned EMDs, the lensing optical depth for a given FRB can be written as,

$$\tau(f_{\text{PBH}}, z_S, w, \mathbf{p}_{\text{mf}}) = \int dm \int_0^{z_S} d\chi(z_L) (1 + z_L)^2 n_L(f_{\text{PBH}}) \sigma(m, z_L, z_S, w) P(m, \mathbf{p}_{\text{mf}}), \quad (14)$$

where \mathbf{p}_{mf} represents the set of parameters in the mass function. Obviously, the optical depth for the MMD of PBHs Eq. 7 can be derived by combining Eq. 14 and Eq. 9.

Intuitively, these constraints can be understood by following the equivalent mass formalism introduced in (Bellomo et al. 2018; Laha 2020). In this formalism, one finds a single lens mass which represents the full effect of the EMD. This formalism is valid for any EMD and we can use it to recast the limits on the PBHs that had been derived for MMD. We can calculate the equivalent mass for the EMDs by equating the expressions for the integrated optical depth with appropriate changes:

$$\int dz_{\text{sm}} \tau(M_{\text{PBH}}^{\text{eq}}, f_{\text{PBH}}^{\text{MMD}}, z_{\text{sm}}, w) N(z_{\text{sm}}) = \int dz_{\text{se}} \tau(f_{\text{PBH}}^{\text{EMD}}, z_{\text{se}}, w, \mathbf{p}_{\text{mf}}) N(z_{\text{se}}), \quad (15)$$

where the equivalent mass is denoted by $M_{\text{PBH}}^{\text{eq}}$ when $f_{\text{PBH}}^{\text{MMD}} = f_{\text{PBH}}^{\text{EMD}}$ ($f_{\text{PBH}}^{\text{MMD}}$ and $f_{\text{PBH}}^{\text{EMD}}$ represent the fraction of PBHs when MMD and EMD are used respectively). The redshifts for the MMD and EMD are denoted by z_{sm} and z_{se} , respectively. After deducing the equivalent mass for a given input of EMD, we can then read off the f_{PBH} for that distribution by using Figs. (3,4).

3 CONSTRAINTS FROM THE LATEST FRB OBSERVATIONS

In this section, we first describe the latest FRB data. In addition, we show the constraints on the abundance of PBHs from the latest FRBs observations with both MMD and EMDs taken into account.

3.1 The latest FRB data

At present, there are about 593 publicly available FRBs. This number has significantly increased because of the release of the first CHIME/FRB FRB catalog, which consist of more than five hundred events detected in less than one year (2018 July 25 to 2019 July 1)³ (CHIME/FRB Collaboration, 2021).

³ <https://www.chime-frb.ca/catalog>

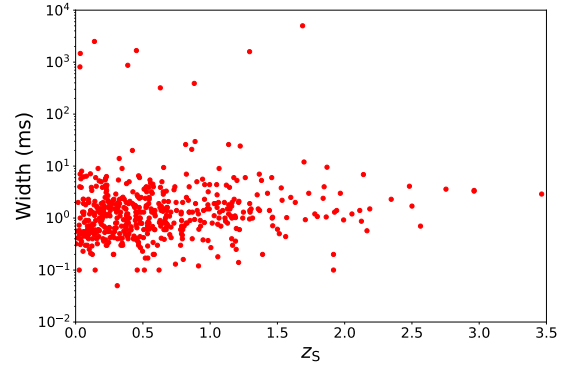


Figure 1. Two-dimensional distribution of inferred redshifts and widths for the latest 593 FRBs.

For a detected FRB, one of the most important observational features is the DM, which is measured from the delayed arrival time of two photons with different frequencies. Even though the first several bursts were poorly localized (Lorimer et al. 2007; Thornton et al. 2013), their cosmological origin was inferred from their extremely excess observed DMs compared with Milky Way DM contributions in the same directions. As expected, their extragalactic origin was soon confirmed by the localization of the first repeater FRB 121102 to a dwarf galaxy at $z \sim 0.19$ (Tendulkar et al. 2017; Chatterjee et al. 2017; Marcote et al. 2017). As a result, the distance and redshift of a detected FRB can be approximately estimated from its observed DM which is usually decomposed into the following four ingredients,

$$\text{DM} = \frac{\text{DM}_{\text{host}} + \text{DM}_{\text{src}}}{1 + z} + \text{DM}_{\text{IGM}} + \text{DM}_{\text{MW}}, \quad (16)$$

where DM_{host} and DM_{src} represent DM from host galaxy and local environment, respectively. Here, we adopt the minimum inference of redshift for all host galaxies, which corresponds to the maximum value of $\text{DM}_{\text{host}} + \text{DM}_{\text{src}}$ to be $200 \text{ pc}^3/\text{cm}^3$. DM_{MW} is the contribution from the Milky Way. In addition, the intergalactic medium (IGM) contribution DM_{IGM} is closely related to the redshift or distance of the source and the baryon content of the universe. The $\text{DM}_{\text{IGM}} - z$ relation is given by (Deng & Zhang 2014) and it is approximately expressed as $\text{DM}_{\text{IGM}} \sim 855z \text{ pc}^3/\text{cm}^3$ by considering the fraction f_{IGM} of baryon in the IGM to $f_{\text{IGM}} = 0.83$ and the He ionization history (Zhang 2018). DM and redshift measurements for several localized FRBs suggested that this relation is statistically favored by observations (Li et al. 2020). Duration of FRB is also an important observational feature for determining the mass range of PBHs to be constrained from the lensing effect of these bursts, so we collect the inferred redshifts and pulse widths of all currently available FRBs and present them in Fig. 1.

Moreover, for the latest 593 available FRBs, especially those with multiple peaks, we have carefully checked their light curves, intrinsic structures, and dynamic spectra, and no candidate with strong evidence of lensing effect has been found (Zhou et al. 2021). In our following analysis, we derive constraints on the abundance of PBHs from this null search result of lensed signals with different mass distributions taken into consideration.

3.2 Constraints from the latest data

We first derive constraints on the abundance of PBHs from this null search result of lensed FRBs in the framework of MMD. Each $(M_{\text{PBH}}, f_{\text{PBH}})$ corresponds to an expected number of lensed FRB signals according to Eqs. (7, 8). Since no lensed FRB event has been found in the current data, the curve in the $(M_{\text{PBH}}, f_{\text{PBH}})$ parameter space that predict one detectable lensed FRB, as shown in panel (a) of Fig. 2, is disfavored at 63% confidence level (assuming Poisson events and uniform prior on the summed lensing optical depth). In the $\lesssim 10 M_{\odot}$ low-mass end, f_{PBH} is unconstrained because of the time delay (Δt) resolution limit; For the mass range $10\text{--}10^3 M_{\odot}$, the constraint gradually improves towards larger mass end, where the Δt resolution impact diminishes. In the $\gtrsim 10^3 M_{\odot}$ large-mass end, the constraint on f_{PBH} saturates to $\lesssim 8.6\%$ (63% confidence level). The overall result is improved compared to the constraint on the compact objects presented in Liao et al. (2020).

Next, we derive constraints on f_{PBH} assuming that masses of PBHs follow the extended power-law distribution, and the results is shown in panel (b) of Fig. 2. Here, we assume M_{max} in the extended power-law mass function to be $M_{\text{max}} = 10^3 M_{\odot}$ (or $10^4 M_{\odot}$) and vary the minimum value, M_{min} from $1 M_{\odot}$ to $999 M_{\odot}$ (or $9999 M_{\odot}$). In addition, we set three values for the parameter γ , i.e. 0, -0.5 , and -1 . Analogously, each $(M_{\text{min}}, f_{\text{PBH}})$ corresponds to an expected number of lensed FRB signals according to Eqs. (8, 14). Again we show the curves that predict one detectable lensed signal as references. In this model, the constraints from larger mass end is extrapolated to the low-mass end by the assumed power-law form. The $\gamma = 0$ case corresponds to a flatter mass distribution, which leads to a better extrapolation efficiency. Similar to the MMD model, the $M_{\text{max}} = 10^3 M_{\odot}$ cases are limited by the Δt resolution limit, and hence f_{PBH} are typically worse constrained than the $M_{\text{max}} = 10^4 M_{\odot}$ cases.

For the log-normal mass distribution, the results of the projected constraints on f_{PBH} is shown in the lower left panel of Fig. 2. We set the width of mass spectrum σ to be several typical values: 0.5, 1, 2, and 3. In addition, we assume the value of the peak mass m_c varies from $1 M_{\odot}$ to $10^4 M_{\odot}$. Similarly, each (m_c, f_{PBH}) corresponds to an expected number of lensed FRB signals according to Eqs. (8, 14), and the area in the (m_c, f_{PBH}) parameter space above the curve which predicts one detectable lensed signal should be disfavored because no lensed FRB event has been found in the current data. For a fixed $m_c \gtrsim 45 M_{\odot}$, a broader mass distribution (larger σ) typically leads a worse constraint on f_{PBH} . This is because more Δt -unresolved (low- M_{PBH}) lensing cases are allowed in a broader distribution. This argument, however, cannot be applied if $m_c \lesssim 45 M_{\odot}$, where a broader mass distribution also brings in more $45 M_{\odot}$ samples that are better constrained than the $M_{\text{PBH}} = m_c$ case. We observe numerically that this effect is not competitive enough to beat the previous mentioned effect that extension to lower-mass end worsens the constraint.

For the critical collapse mass distribution, the constraints on f_{PBH} from the latest FRB observations is shown in the lower right panel of Fig. 2. In this scenario, the value of α , which is a universal exponent relating to the critical collapse of radiation, is assumed to be 1.5, 2, 2.5, and 3 and the mass-scale M_f is assumed to vary from $1 M_{\odot}$ to $10^4 M_{\odot}$. Similar

to the above-mentioned three cases, each (M_f, f_{PBH}) corresponds to an expected number of lensed FRB signals according to Eqs. (8, 14). Since no lensed signal has been found in the current data, in the (M_f, f_{PBH}) parameter space, the region above the curve that predicts one detectable lensed signal is disfavored. For large α 's, this mass distributions, and hence the constraints on f_{PBH} , are all very close to the MMD case. For a smaller α , the mass distribution is flatter in the small mass range. Similar to the log-normal case, for a flatter mass distribution two effects compete. The outreach to the larger-mass end improves the constraint on f_{PBH} , whereas the extension to the lower-mass end worsens the constraint. The numeric result here suggests that, in contrary to the log-normal case, here flattening of distribution slightly improves the constraint.

4 FORECASTS

Although the current constraints from the latest observations are weak due to a small number of FRBs available at this moment, and this work is more like a proof of concept, more stringent limits on PBH properties will be achieved from upcoming observations of this new and promising probe, owing to rapid progress in the FRB observation community.

It is expected that upcoming wide field radio surveys, especially CHIME (CHIME/FRB Collaboration, 2018), ASKAP (Bhandari et al. 2019), DSA-2000 (Hallinan et al. 2019), will detect a large number of FRBs, i.e. $\sim 10^4$ per year. In addition, several other telescopes, like the Five-hundred-meter Aperture Spherical Telescope (FAST) (Zhang 2018), the Upgraded Giant Metrewave Radio Telescope (Bhattacharyya 2018), Ooty Wide Field Array (Bhattacharyya 2018), UT-MOST (Bailes et al. 2017), HIRAX (Weltman & Walters 2017), and APERITIF (Maan & Leeuwen 2017) will revolutionize the fields of FRB observations and applications.

If we accumulate a considerable number of FRBs with redshifts satisfying $N(z_S)$ distribution in the near future, the integrated optical depth of all these bursts $\bar{\tau}(M_{\text{PBH}}, f_{\text{PBH}}, w)$ is,

$$\bar{\tau}(M_{\text{PBH}}, f_{\text{PBH}}, w) = \int dz_S \tau(M_{\text{PBH}}, f_{\text{PBH}}, z_S, w) N(z_S). \quad (17)$$

Consequently, the expected number of lensed FRBs is,

$$N_{\text{lensed FRB}} = (1 - e^{-\bar{\tau}(M_{\text{PBH}}, f_{\text{PBH}}, w)}) N_{\text{FRB}}. \quad (18)$$

In our following analysis, we use two realistic redshift distributions $N(z)$ of FRBs to make improved forecasts, i.e. the constant-density redshift distribution (CRD) $N_{\text{CRD}}(z)$ and the star-formation redshift distribution (SRD) $N_{\text{SRD}}(z)$. Specifically, the CRD is expressed as (Muñoz et al. 2016; Laha 2020; Oppermann et al. 2016),

$$N_{\text{CRD}}(z) = \mathcal{N}_c \frac{\chi^2(z) e^{-d_L^2(z)/[2d_L^2(z_{\text{cut}})]}}{(1+z)H(z)}, \quad (19)$$

where \mathcal{N}_c is a normalization factor to ensure that $N_{\text{CRD}}(z)$ integrates to unity, $d_L(z)$ is the luminosity distance, in this work computed with Planck best-fit Λ CDM model (Planck Collaboration, 2020), and z_{cut} is a Gaussian cutoff in the FRB redshift distribution due to an instrumental signal-to-noise threshold. The SRD can be written as (Muñoz et al.

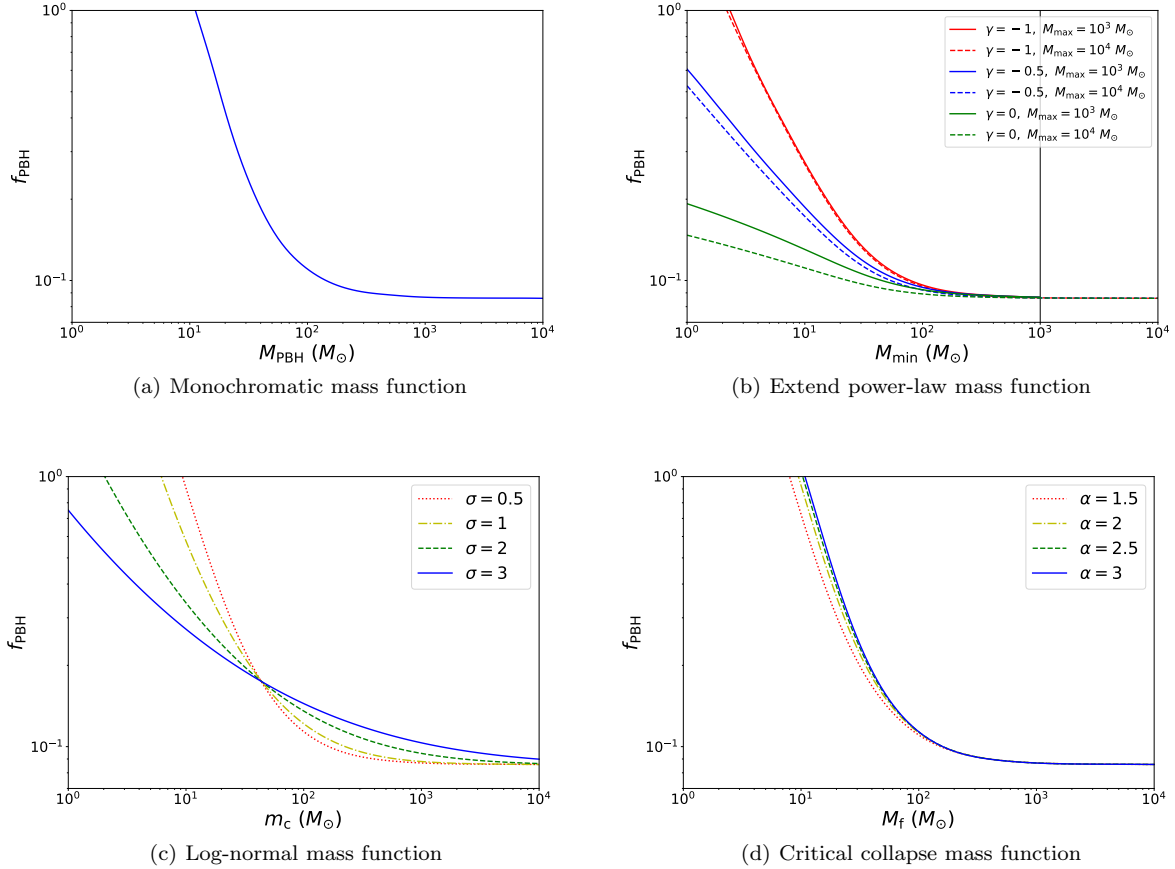


Figure 2. **Upper left:** Constraints on the upper limits of fraction of dark matter in the form of PBHs with the MMD function from the fact that no lensed signal has been found in 593 FRBs data. **Upper right:** Same as the upper left panel but for the extend power-law distribution with $\gamma = 0, -0.5,$ and -1 and a fixed M_{\max} . Solid lines represent the constraints of $M_{\max} = 10^3 M_{\odot}$ and dashed lines represent the constraints of $M_{\max} = 10^4 M_{\odot}$. **Lower left:** Same as the upper left panel but for the log-normal distribution with $\sigma = 0.5, 1, 2,$ and 3 . **Lower right:** Same as the upper left panel but for the critical collapse distribution for $\alpha = 1.5, 2, 2.5,$ and 3 .

2016; Laha 2020; Caleb et al. 2016):

$$N_{\text{SRD}} = \mathcal{N}_s \frac{\dot{\rho}_*(z) \chi^2(z) e^{-d_L^2(z)/[2d_L^2(z_{\text{cut}})]}}{(1+z)H(z)}, \quad (20)$$

where \mathcal{N}_s is the normalization constant which is determined from $\int dz N_{\text{SRD}}(z) = 1$, and

$$\dot{\rho}_*(z) = h \frac{a + bz}{1 + (z/s)^d}, \quad (21)$$

where $a = 0.017, b = 0.13, s = 3.3, d = 5.3,$ and $h = 0.7$.

In this section, we firstly present forecasts of constraints on PBH properties from upcoming FRBs assuming two redshift distributions (CRD and SRD) of them. Moreover, we compare the forecasts with the constraints from GW observations to study the possibility of joint constraints on PBHs from near future multi-messenger observations.

4.1 Forecast with different mass function

In Fig. 3, we demonstrate the constraints on dark matter fraction in the form of PBHs when the MMD is considered. These results are similar to what were obtained in (Laha 2020; Muñoz et al. 2016). The solid lines and dashed lines

represent the constraints on f_{PBH} from 10^4 FRBs with CRD and SRD, respectively. Given that the temporal width of the bursts varies and the presence of sub-bursts, we estimate that the wide range of $\overline{\Delta t}$ will represent a satisfactory projection into the potential constraints that a future survey like CHIME can achieve. Therefore, we assume the average widths of FRBs as follows: $\overline{\Delta t} = 0.1, 0.3, 1,$ and 3 ms. As shown in Fig. 3, a smaller value of $\overline{\Delta t}$ allows one to probe lower lens masses in the $M_{\text{PBH}} - f_{\text{PBH}}$ plane. By using 10^4 FRBs, the abundance of PBH f_{PBH} at large mass that can be asymptotically constrained to $\sim 0.7\%$ and $\sim 0.5\%$ assuming the CRD and the SRD, respectively. In addition, compared to the CRD, constraints from FRBs with redshifts satisfying the SRD are slightly more stringent because SRD generally predicts more high-redshift FRBs.

Next, we derive the projected constraints on f_{PBH} with $N_{\text{FRB}} = 10^4$ assuming that mass of PBHs follow three different distributions. Moreover, we also assume two different redshift distributions for FRBs (CRD and SRD) and two representative average widths of them ($\overline{\Delta t} = 0.1,$ and 1 ms). Constraints on different parameter spaces are shown in Figs. (4, 5, 6). In addition, all the white regions in the Figs from the forecast with EMDs represent that f_{PBH} is more than 1. In

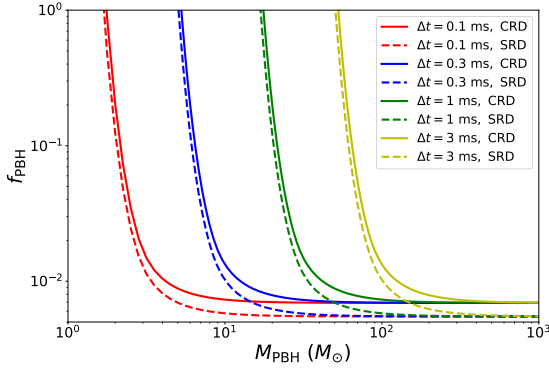


Figure 3. Constraints on the upper limits of the fraction of dark matter in the form of PBH with the MMD from the fact that no lensed signal has been found in the upcoming 10^4 FRBs with average values of the critical time, $\overline{\Delta t} = 0.1, 0.3, 1,$ and 3 ms. The solid lines and dashed lines represent results when the CRD and SRD is considered, respectively.

Fig. 4, we assume that the maximum value of the extended power-law mass function $M_{\max} = 10^3 M_{\odot}$ and vary the minimum value M_{\min} from $1 M_{\odot}$ to $100 M_{\odot}$. The regions where 10% and 1% of dark matter consists of PBHs are denoted in Fig. 4 by the red solid lines. The dependence of the results on the power-law slope γ is similar to the real-data case, and $\overline{\Delta t}$ and SRD/CRD of FRBs all affect the results in the same way as in the MMD case.

The forecasting constraints for the log-normal mass function are shown in Fig. 5. We assume that the value of m_c varies from $1 M_{\odot}$ to $100 M_{\odot}$ and σ is greater than 0.1. The regions where 10% and 1% of dark matter can consist of PBHs are denoted by the red solid lines. Unlike the real-data case, here we probe a lower mass range. The quantitative competition between the two above-mentioned effects of broadening the mass distribution, and hence the dependence of the f_{PBH} constraint on σ , is more complicated.

For the critical collapse mass function, the constraints with same $\overline{\Delta t}$ and redshift distributions of FRBs are shown in Fig. 6. The contour lines where 10% and 1% of dark matter from PBHs are marked by the red solid lines. Similar to the real-data case, the constraint on f_{PBH} is sensitive to M_f , but insensitive to α .

4.2 Comparisons with GW constraints

Detection of GW bursts from merges of compact object binaries is one of the most promising ways to study the mass distribution of PBHs. Constraints on the PBH scenario from the GWTC-1/GWTC-2 catalog have been widely studied via the Bayesian inference method and in the EMDs framework (Chen et al. 2019; Wu 2020; Hütsi, et al. 2021; Wong et al. 2021; De Luca et al. 2020). Meanwhile, as suggested in this paper, the abundance of PBHs in the mass range $1\text{--}100 M_{\odot}$ also can be well constrained from the gravitational lensing effect of upcoming FRBs. Therefore, it is interesting to compare constraints on the PBH properties from GW detection with the ones obtained from FRBs observations. This comparison will be helpful for exploring the possibility

of jointly constraining PBH scenarios from newly-developing multi-messenger observations.

For consistency and illustration, here we apply the commonly used log-normal mass distribution to calculate the co-moving merger rate density (Chen & Huang 2018)

$$R_{12}(z, m_1, m_2, \sigma, m_c) = 3.9 \cdot 10^6 \left(\frac{t(z)}{t_0} \right)^{-\frac{34}{37}} f^2 (f^2 + \sigma_{\text{eq}}^2)^{-\frac{21}{74}}$$

$$\min \left(\frac{P(m_1, \sigma, m_c)}{m_1}, \frac{P(m_2, \sigma, m_c)}{m_2} \right) (m_1 m_2)^{\frac{3}{37}} (m_1 + m_2)^{\frac{36}{37}}$$

$$\left(\frac{P(m_1, \sigma, m_c)}{m_1} + \frac{P(m_2, \sigma, m_c)}{m_2} \right), \quad (22)$$

where t_0 is the age of the universe, and σ_{eq} is the variance of density perturbations of the rest dark matter on scale of order $\mathcal{O}(10^0 \sim 10^3) M_{\odot}$ at radiation-matter equality. Here f is the total abundance of PBHs in non-relativistic matter, and relates to the fraction of PBHs via $f_{\text{PBH}} \equiv \Omega_{\text{PBH}}/\Omega_{\text{CDM}} \approx f/0.85$. Integrating over the component masses in the merger rate density, we can obtain the merger rate as a function with respect to redshift,

$$R(z) = \int R_{12}(z, m_1, m_2, \sigma, m_{r,mc}) dm_1 dm_2. \quad (23)$$

The local merger rate is defined as $R_0 \equiv R(z=0)$. In this paper, the local merger rate of PBHs is assumed as 10, 40, 70, and 100 $\text{Gpc}^{-3}\text{yr}^{-1}$, respectively, to infer the fraction of dark matter in the form of PBHs. Then this inferred f_{PBH} will be compared with the constraints from FRB observations. As shown in Fig. 7, we assume that, for the log-normal mass distribution in the merger rate Eq. 23, m_c is in the range of $10\text{--}30 M_{\odot}$ and σ ranges from 0.1 to 2. These priors are roughly consistent with the parameter space constrained from the latest GW data. It is suggested that, for the assumption $R_0 = 10 \text{ Gpc}^{-3}\text{yr}^{-1}$, f_{PBH} is estimated to be $< 0.1\%$, whereas for the assumption $R_0 = 100 \text{ Gpc}^{-3}\text{yr}^{-1}$, f_{PBH} is estimated to be $< 0.3\%$. However, as shown in Fig. 5, the upper limits of f_{PBH} is approximately constrained to be 0.5% (0.7%) from null search result of lensing copies in 10^4 FRBs when the SRD (CRD) and $\overline{\Delta t} = 0.1$ ms is assumed. Obviously, constraints on the upper limit of f_{PBH} from the null search result of $N_{\text{FRB}} = 10^4$ FRBs is slightly weaker than the one estimated from GW observations. That is, the constrained regions in the log-normal mass distribution parameter space from observations of these two kind messengers are hardly to overlap. Therefore, in this paper we make a further assumption of a null search of lensing phenomenon in 10^5 FRBs with value of the critical time $\overline{\Delta t} = 0.1$, and 1 ms with two above-mentioned redshift distributions. As shown in Fig. 8, the contour lines representing 0.3% and 0.2% of dark matter in the form of PBHs are denoted by the red solid lines. It is found that, there are considerable areas in the parameter space with the upper limits of f_{PBH} less than 0.1% when $\overline{\Delta t} = 0.1$ ms is assumed. In contrast, for the assumption $\overline{\Delta t} = 1$ ms, areas in the parameter space with the upper limits of f_{PBH} less than 0.1% disappear. However, most of the upper limits of f_{PBH} in the parameter spaces are less than 0.3%. Generally speaking, in the parameter space, there are considerable overlap between the constraints from GW observations and a null search of lensing candidate in 10^5 FRBs. This overlap makes it possible to get joint constraints

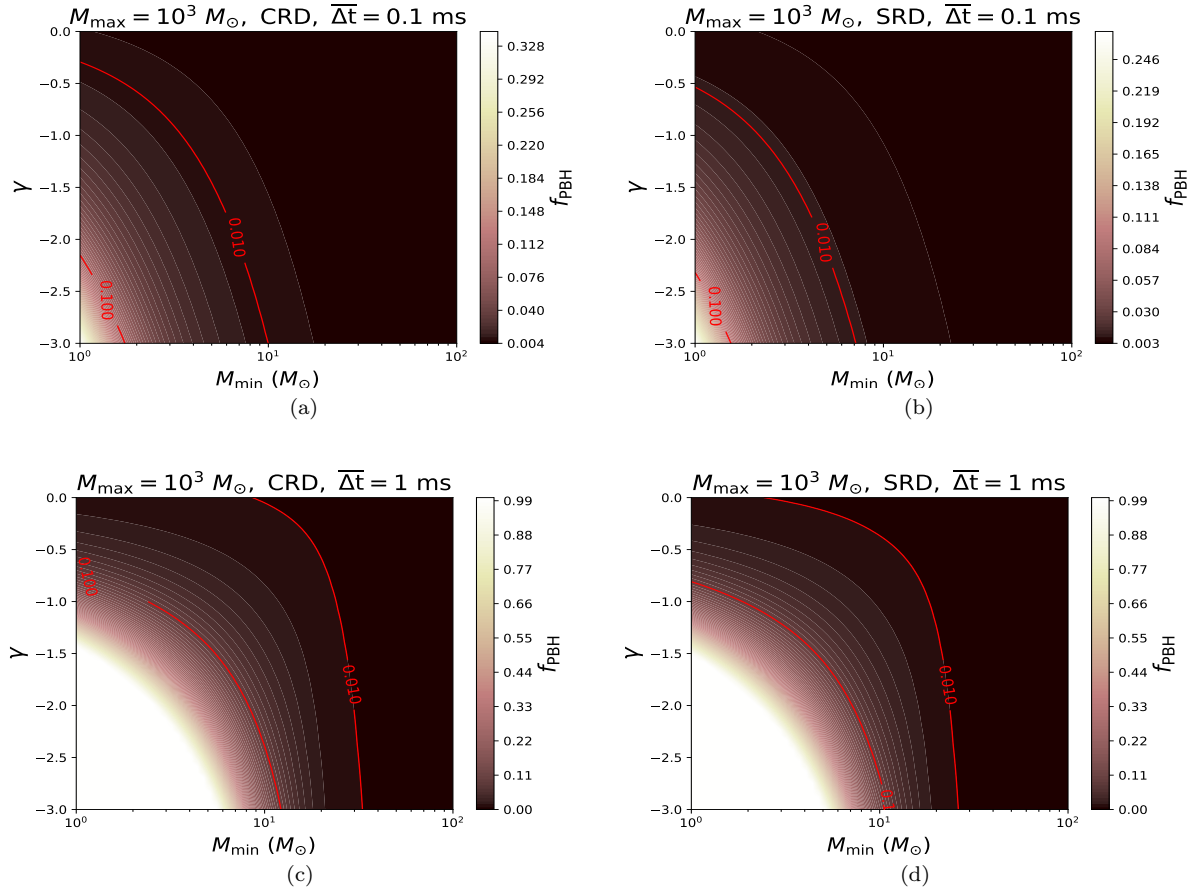


Figure 4. Constraints on the extend power-law mass function with a fixed maximum mass $M_{\max} = 10^3 M_{\odot}$ from a null search result of lensing echoes in 10^4 FRBs. In addition, we assume that M_{\min} ranges from $1 M_{\odot}$ to $100 M_{\odot}$ and γ is from -3 to 0 . **Upper left:** Results correspond to the assumptions that FRBs follow the constant-density redshift distribution and have average value of the critical time $\overline{\Delta t} = 0.1$ ms. **Upper right:** Same as the upper left panel but for the assumption that FRBs follow the star-formation redshift distribution. **Lower left:** Same as the upper left panel but for the assumption that FRBs have average value of the critical time $\overline{\Delta t} = 1$ ms. **Lower right:** Same as the upper left panel but for the assumptions that FRBs follow the star-formation redshift distribution and have average value of the critical time $\overline{\Delta t} = 1$ ms.

on the properties of stellar mass PBHs from the upcoming multi-messenger observations.

5 CONCLUSIONS AND DISCUSSIONS

The recent detection of GW from binary black hole merger have caused great interests in stellar mass PBHs. Consequently, detection of GW has been deemed as one of the most promising ways to examine the nature of PBHs. Meanwhile, in the electromagnetic domain, gravitational lensing effect of prolific transients with millisecond duration, e.g. FRBs, has been proposed as one of the cleanest probes for exploring properties of PBHs in the mass range $1 - 100 M_{\odot}$. In this paper, we first derive constraints on the abundance of PBH from the latest FRB observations and obtain that, for $M_{\text{PBH}} \gtrsim 10 M_{\odot}$ an upper bound of f_{PBH} can be achieved. The 1σ bound saturates to $\sim 10\%$ in the large-mass ($\gtrsim 10^3 M_{\odot}$) end. This current constraint is weak but also of great significance in providing complementary information from observations of the newly discovered transient. Moreover, we investigate the dependence of results on the mass functions of PBH by

taking three extended mass distributions, which are related to well-defined theoretical motivations, into consideration. It appears that, in general, the latest FRB observations yield to consistent constraints on the upper limit of f_{PBH} for different mass distribution scenarios.

In addition to the constraints from currently available FRBs, we forecast the constraining power of upcoming FRB observations on the properties of PBHs by taking possible impact factors, such as the mass distribution function and the redshift distribution of FRBs, into account. First, we conservatively assume a sample of 10^4 FRBs, which is probably to be detected by the upcoming wide-field radio arrays (like DSA-2000) in one year. We find that, for most cases, the upper limit of f_{PBH} at large mass can be asymptotically constrained to $\sim 0.7\%$ from the null search of lensing event in 10^4 FRBs. Meanwhile, we also estimate the abundance of PBHs from GW observations. Our results indicate that, compared with upcoming 10^4 FRBs, current GW observations can present much more stringent constraints on the abundance of PBH. Therefore, we further investigate forecasting implications from 10^5 FRBs which might be accumu-

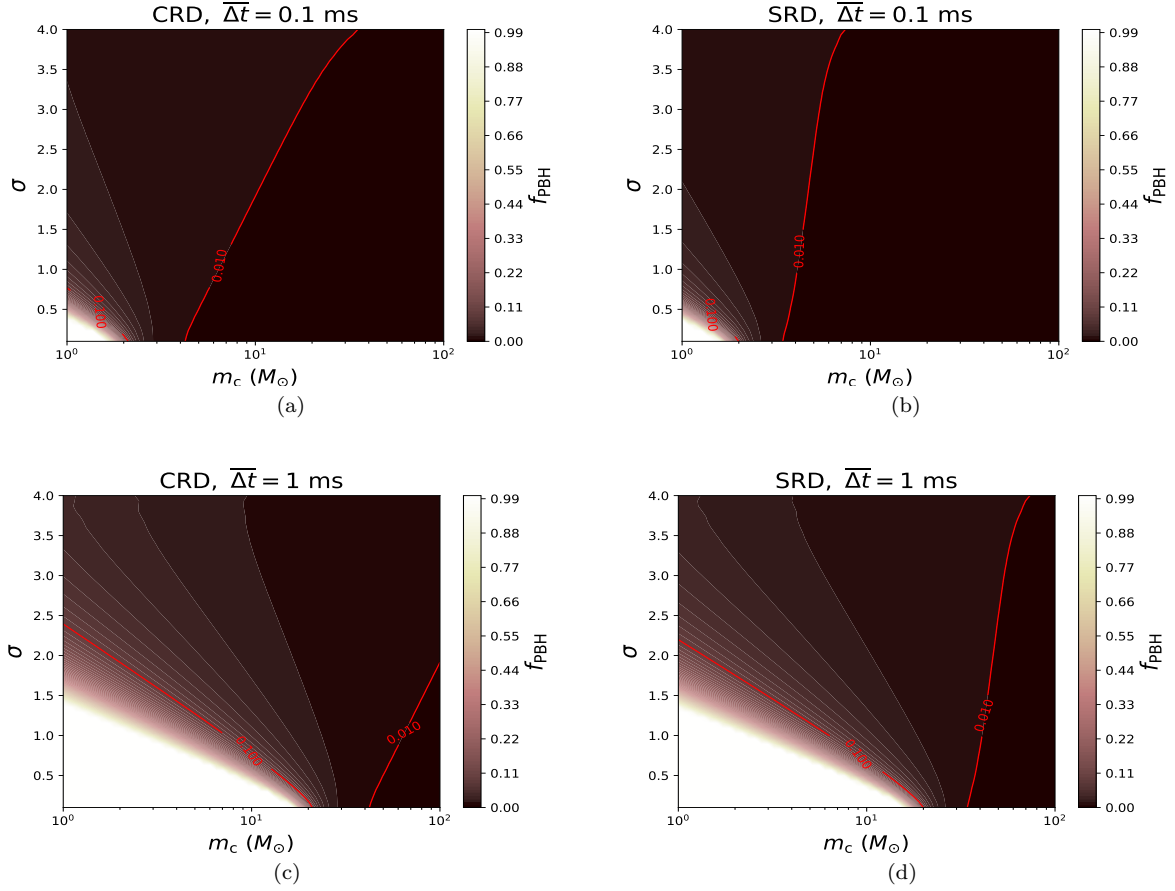


Figure 5. Same as Fig. 4 for the log-normal mass function with two parameters (σ, m_c). In addition, we assume that m_c ranges from $1 M_\odot$ to $100 M_\odot$ and σ is from 0.1 to 4.0, which are roughly consistent with the estimation derived from GW observations.

lated in several years and find that, in the framework of the log-normal mass distribution, the upper limit of f_{PBH} can be asymptotically constrained to $\sim 0.1\%$. This constraint is close to the one estimated from GW observations. As a result, in the parameter space of the mass distribution, there would be significant overlap between areas constrained from FRB observations and the ones from GW detection. This merit is of great importance for the possibility of deriving joint constraints on the abundance and mass distribution of PBHs from the combination of forthcoming complementary multimessenger observations. It is foreseen that these joint constraints will be very helpful for exploring the nature of PBHs in the stellar mass range, or even their formation mechanisms relating to the evolution theories of the early universe.

6 ACKNOWLEDGEMENTS

We would like to thank Zu-Cheng Chen and You Wu for their helpful discussions about estimation for mass distribution of PBHs from GW observations. This work was supported by the National Natural Science Foundation of China under Grants Nos. 11920101003, 11722324, 11603003, 11633001, 12073088, and U1831122, Guangdong Major Project of Basic and Applied Basic Research (Grant No. 2019B030302001), the Strategic Priority Research Program of the Chinese

Academy of Sciences, Grant No. XDB23040100, and the Interdiscipline Research Funds of Beijing Normal University.

REFERENCES

- Abbott, B. P., Abbott, R., Abbott, T. D., et al., 2016, PRL, 116, 061102
- Aghanim, N., Akrami, Y., Ashdown, M., et al., 2020, A&A 641, A6
- Alcock, C., Allsman, R. A., Alves, D. R., et al., 2001, ApJ, 550, L169
- Ali-Haïmoud Y., Kamionkowski M., 2017, PRD, 95, 043534
- Aloni, D., Blum, K., Flauger, R., 2017, JCAP, 05, 017
- Ashoorioon, A., Rostami, A., Firouzjaee, J. T., 2021, JHEP, 07, 087
- Bailes, M., et al., 2017, Pub. Astron. Soc. Aust. 34, e045
- Bellomo, N., Bernal, J. L., Raccanelli, A., Verde, L., 2018, JCAP, 01, 004
- Beniamini, P., Kumar, P., Ma, X.-C., Quataert, E., 2021, MNRAS, 502, 4
- Bernal, J. L., Bellomo, N., Raccanelli, A., Verde, L., 2017, JCAP, 10, 052
- Bhandari, S., et al., 2019, MNRAS, 486, 70
- Bhattacharyya, S., 2018, J. Astrophys. Astron. 39, 47
- Bhattacharyya, M., Kumar, P., Linder, E. V., 2021, PRD, 10, 103526
- Bird, S., et al., 2016, PRL, 116, 201301

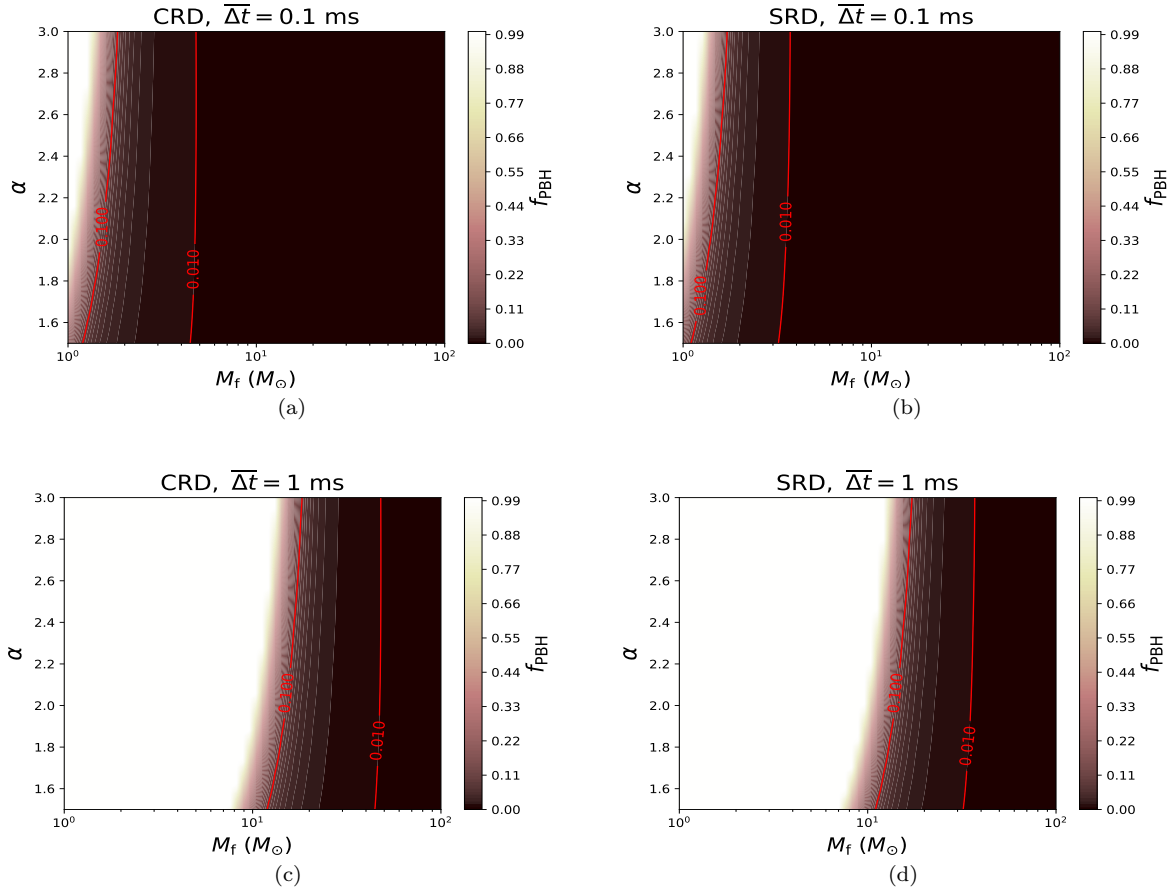


Figure 6. Same as Fig. 4 but for the critical collapse mass function with two parameters (α, M_f). In addition, we assume that M_f ranges from $1 M_\odot$ to $100 M_\odot$ and α is from 1.5 to 3.

Bochenek, C. D., Ravi, V., Belov, K. V., et al., 2020, *Nature*, 587, 59
 Brandt, T. D., 2016, *ApJ*, 824, L31
 Caldwell, R. R., Chamblin, A., Gibbons, G. W., 1996, *PRD*, 53, 7103
 Caleb, M., Flynn, C., Bailes, M., et al., 2016, *MNRAS*, 458, 708
 Carr, B. J., Hawking, S. W., 1974, *MNRAS*, 168, 399
 Carr, B. J., 1975, *ApJ*, 201, 1
 Carr, B. J., Lidsey, J. E., 1993, *PRD*, 48, 543
 Carr, B. J., Gilbert, J. H., Lidsey, J. E., 1994, *PRD*, 50, 4853
 Carr, B. J., Kohri, K., Sendouda, Y., Yokoyama, J., 2010, *PRD*, 81, 104019
 Carr, B. J., Kohri, K., Sendouda, Y., Yokoyama, J., 2016, *PRD*, 94, 044029
 Carr, B., Raidal, M., Tenkanen, T., Vaskonen, V., Veermäe, H., 2017, *PRD*, 96, 023514
 Champion, D. J., Petroff, E., Krameret, M., et al., 2016, *MNRAS*, 460, L30
 Chatterjee, S., Law, C. J., Wharton, R. S., et al., 2017, *Nature*, 54, 58
 The CHIME/FRB Collaboration., 2018, *ApJ* 863 48
 CHIME/FRB Collaboration., 2020, *Nature*, 587, 54
 CHIME/FRB Collaboration., 2021, arXiv: 2106.04352
 Chen, C., Cai, Y.-F., 2019, *JCAP*, 10, 068
 Chen, L., Huang, Q.-G., Wang, K., 2016, *JCAP*, 1612, 044
 Chen, Z.-C., Huang, Q.-G., 2018, *ApJ*, 864, 61
 Chen, Z.-C., Huang, F., Huang, Q.-G., 2019, *ApJ*, 871, 97
 Chen, Z.-C., Yuan, C., Huang, Q.-G., 2020, *PRL*, 124, 251101

Chen, Z.-C., Huang, Q.-G., 2020, *JCAP*, 08, 039
 Clark, S., Dutta, B., Gao, Y., Ma, Y.-Z., Strigari, L. E., 2018, *PRD*, 98, 043006
 Clesse, S., García-Bellido, J., 2015, *PRD*, 92, 023524
 Clesse, S., García-Bellido, J., 2017, *Phys. Dark Universe*, 18, 105
 Connor, L., et al., 2016, *MNRAS*, 460, 1054
 Cordes, J. M., Chatterjee, S., 2019, *ARAA*, 57, 417
 Dai, L., Lu, W.-B., 2017, *ApJ*, 847, 1
 Dasgupta, B., Laha, R., Ray, A., 2020, *PRL*, 125, 101101
 De Luca, V., Franciolini, G., Pani, P., Riotto, A., 2020, *JCAP*, 06, 044
 Deng, W., Zhang, B., 2014, *ApJL*, 783, L35
 DeRocco, W., Graham, P. W., 2019, *PRL*, 123, 251102
 Diego, J. M., 2020, *PRD*, 101, 123512
 Fu, C.-J., Wu, P.-X., Yu, H.-W., 2019, *PRD*, 100, 063532
 Gao, H., Li, Z.-X., Zhang, B., 2014, *ApJ*, 788, 189
 Graham, P. W., Rajendran, S., Varela, J., 2015, *PRD*, 92, 063007
 Green, A. M., 2016, *PRD*, 94, 063530
 Green, A. M., Kavanagh, B. J., 2021, *J.Phys.G*, 48, 043001
 Griest, K., Cieplak, A. M., Lehner, M. J., 2013, *PRL*, 111, 181302
 Halder, A., Banerjee, S., 2021, *PRD*, 103, 063044
 Hallinan, G., et al., 2019, arXiv:1907.07648
 Hawking, S. W., 1971, *MNRAS*, 152, 75.
 Hawking, S. W., Moss, I. G., Stewart, J. M., 1982, *PRD*, 26, 2681
 Hawking, S. W., 1989, *PLB*, 231, 237
 Hektor, A., Hutsi, G., Marzola, L., Raidal, M., Vaskonen, V., Veermäe, H., 2018, *PRD* 98, 023503
 Hogan, C. J., 1984, *PLB*, 143, 87

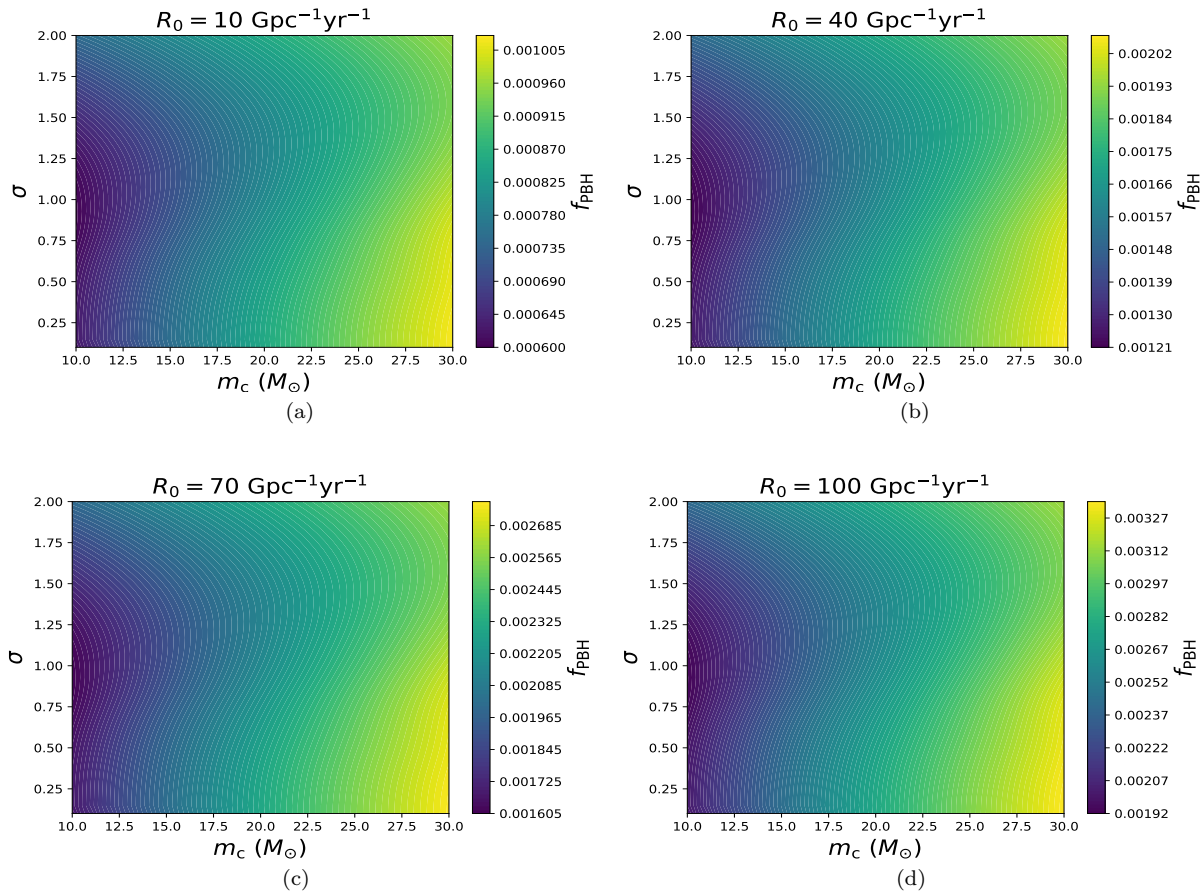


Figure 7. Constraints on the fraction of dark matter in PBHs with the log-normal mass distribution from the latest GW observations. The priors that m_c ranges from $10 M_\odot$ to $30 M_\odot$, and σ is from 0.1 to 2 are considered. Panels (a, b, c, d) represent results when the merger rate of PBHs is assumed as 10, 40, 70, and $100 \text{ Gpc}^{-3}\text{yr}^{-1}$, respectively.

Hütsi, G., Raidal, M., Vaskonen, V., Veermäe, H., 2021, JCAP, 03, 068
 Ji, L.-Y., Kovetz, E. D., Kamionkowski, M., 2018, PRD, 98, 123523
 Kannike, K., Marzola, L., Raidal, M., Veermäe, H., 2017, JCAP, 09, 020
 Koushiappas, S. M., Loeb, A., 2017, PRL, 119, 041102
 Laha, R., 2019, PRL, 123, 251101
 Laha, R., 2020, PRD, 102, 023016
 Laha, R., Muñoz, J. B., Slatyer, T. R., 2020, PRD, 101, 123514
 Li, Z.-X., Gao, H., Ding, X.-H., Wang, G.-J., Zhang, B., 2018, Nat. Comm., 9, 3383
 Li, Z.-X., Gao, H., Wei, J.-J., et al., 2019, ApJ, 876, 146
 Li, Z.-X., Gao, H., Wei, J.-J., Yang, Y.-P., Zhang, B., Zhu, Z.-H., 2020, MNRAS, 496, L28
 Liao, K., Zhang, S.-B., Li, Z.-X., Gao, H., 2020, ApJL, 896, L11
 Liao, K., Tian, S.-X., Ding, X.-H., 2020, MNRAS, 495, 2002
 Lin, L., Zhang, C., Wang, P., et al., 2020, Nature, 587, 63
 Linder, E. V., 2020, PRD, 101, 103019
 Lorimer, D. R., Bailes, M., McLaughlin, M. A., Narkevic, D. J., Crawford, F., 2007, Science, 318, 777
 Maan Y., Leeuwen, J. V., 2017, arXiv:1709.06104
 Macquart, J. -P., Prochaska, J. X., McQuinn, M., et al., 2020, Nature, 581, 391
 Marcote, B., Paragi, Z., Hessels, J. W. T., et al., 2017, ApJL, 834, L8
 Mediavilla, E., Jimenez-Vicente, J., Munoz, J. A., VivesArias, H., Calderon-Infante, J., 2017, ApJ, 836, L18

Motohashi, H., Mukohyama, S., Oliosi, M., 2020, JCAP, 03, 002
 Muñoz J. B., Kovetz E. D., Dai L., Kamionkowski M., 2016, PRL, 117, 091301
 Muñoz, J. B., Loeb, A., 2018, PRD, 98, 103518
 Niikura, H., Masahiro, T., Naoki, Y., et al., 2019, Nature Astronomy, 3, 524.
 Niikura, H., Takada, M., Yokoyama, S., Sumi, T., Masaki, S., 2019, PRD, 99, 083503
 Niu, C.-H., Li, D., Luo, R., et al., 2021, ApJL, 909, L8
 Oppermann, N., Connor, L., Pen, U.-L., 2016, MNRAS, 461, 984
 Petroff, E., Bailes, M., Barr, E. D., et al., 2015, MNRAS, 447, 246
 Petroff, E. Barr, E. D., Jameson, A., et al., 2016, PASA, 33, e045
 Pi, S., Zhang, Y.-L., Huang, Q.-G., Sasaki, M., 2018, JCPA, 05, 042
 Prochaska, J. X., Macquart J.-P., McQuinn, M., et al., 2019, Science, 366, 231
 Poulin, V., Serpico, P. D., Calore, F., Clesse, S., Kohri, K., 2017, PRD, 96, 083524
 Sasaki, M., Suyama, T., Tanaka, T., Yokoyama, S., 2016, PRL, 117, 061101
 Sasaki, M., Suyama, T., Tanaka, T., Yokoyama, S., 2018, GReGr, 35, 063001
 Spitler, L. G., Scholz, P., Hessels, J. W. T., et al., 2016, Nature, 531, 202
 Tendulkar, S. P., Bassa, C. G., Cordes, J. M., et al., 2017, ApJL, 834, L7
 Thornton, D., Stappers, B., Bailes, M., et al., 2013, Science, 341,

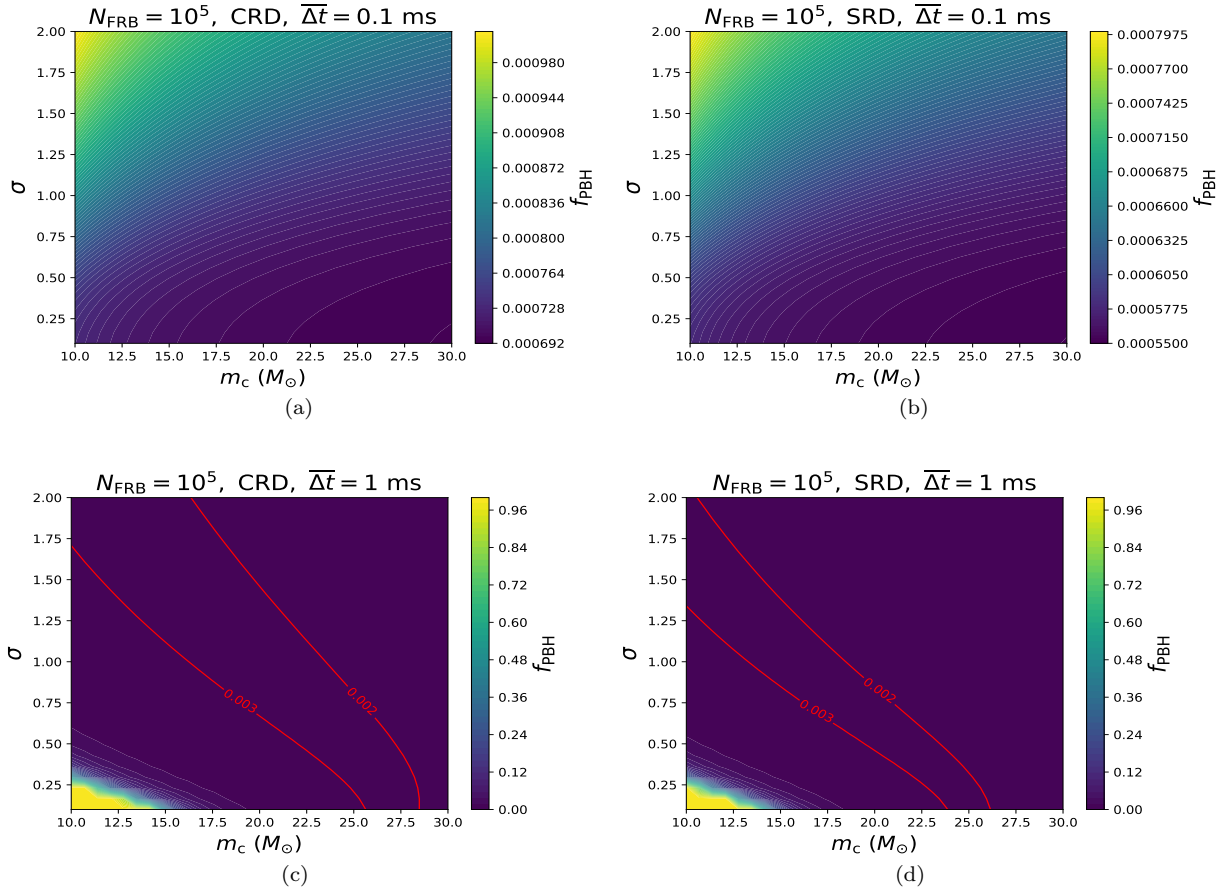


Figure 8. Same as Fig. 5 but for constraints based on the assumption that no lensed signal has been found in 10^5 FRBs. In addition, we assume that m_c ranges from $10 M_\odot$ to $30 M_\odot$ and σ is from 0.1 to 2.0, which are consistent with the parameter space in Fig. 7

53

- Tisserand, P., Guillou, P., Afonso, C., et al., 2007, *A&A* 469, 387
 Urrutia, J., Vaskonen, V., 2021, arXiv:2109.03213
 Walters, A., Weltman, A., Gaensler, B. M., Ma, Y.-Z., Witzemann, A., 2018, *ApJ*, 856, 65
 Wang, S., Wang, Y.-F., Huang, Q.-G., Li, T. G. F., 2018, *PRL*, 120, 191102
 Wang, Y.-K., Wang, F.-Y., 2018, *A&A*, 614, A50
 Wei, J.-J., Gao, H., Wu, X.-F., Mwszaros, P., 2015, *PRL*, 115, 261101
 Weltman, A., Walters, A., Witzemann, A., 2017, <https://inspirehep.net/literature/1671212>
 Wong, Kaze W. K., Franciolini, G., De Luca, V., Baibhav, V., Berti, E., Pani, P., Riotto, A., 2021, *PRD*, 103, 023026
 Wu, X.-F., Zhang, S.-B., Gao, H., et al., 2016, *ApJ*, 822, L15
 Wu, Y., 2020, *PRD*, 101, 083008
 Wucknitz, O., Spitler, L. G., Pen, U. -L., 2020, *A&A*, 645, A44
 Zhang, B., 2018, *ApJL*, 867, L21
 Zhang, B., 2020, *Nature*, 587, 45
 Zhao, Z.-W., Li, Z.-X., Qi, J.-Z., et al., 2020, *ApJ*, 903, 83
 Zhou, B., Li, X., Wang, T., Fan, Y.-Z., Wei, D.-M., 2014, *PRD*, 89, 107303
 Zhou, H., Li, Z.-X., Liao, K., Niu, C.-H., Gao, H., Huang, Z.-Q., Huang, L., Zhang, B., 2021, arXiv: 2109.09251
 Zumalacarrregui, M., Seljak, U., 2018, *PRL*, 121, 141101